Available online at www.sciencedirect.com
SCIENCE DIRECT®
Computational Materials Science 32 (2005) 223–239
COMPUTATIONAL MATERIALS SCIENCE
www.elsevier.com/locate/commatsci

Classification and reconstruction of three-dimensional microstructures using support vector machines

Veeraraghavan Sundararaghavan, Nicholas Zabaras *

Materials Process Design and Control Laboratory, Sibley School of Mechanical and Aerospace Engineering, 188 Frank H.T. Rhodes Hall, Cornell University, Ithaca, NY 14853-3801, USA

Received 27 April 2004; received in revised form 25 June 2004; accepted 22 July 2004

Abstract

Reconstruction of three-dimensional (3D) microstructures is posed and solved as a pattern recognition problem. A microstructure database is used within a support vector machines framework for predicting 3D reconstructions of microstructures using limited statistical information available from planar images. The 3D distributions of the grain size of the reconstructed polyhedral microstructures exhibit qualitative agreement with stereological predictions. Amenability of the approach for studying microstructure–property relationships is shown by comparing the computed properties of reconstructed microstructures with available experimental results. Combination of classification methodology and principal component analysis for effective reduced-order representation of 3D microstructures is demonstrated. The pattern recognition technique discussed uses two-dimensional microstructure signatures to generate in nearly real-time 3D realizations, thus accelerating prediction of material properties and contributing to the development of materials-by-design.

PACS: 92.10.Ns; 42.30.Sy; 87.80.Pa
Keywords: Microstructure reconstruction; Reduced-order representation; Pattern recognition; Support vector machines; Principal component analysis

1. Introduction

Quantitative characterization of three-dimensional material microstructure is essential for understanding the relationships between microstructure and material properties. Three-dimensional microstructures experimentally characterized by combining

* Corresponding author. Tel.: +1 607 255 9104; fax: +1 607 255 1222.
E-mail address: zabaras@cornell.edu (N. Zabaras).
URL: http://www.mae.cornell.edu/zabaras/

0927-0256/$ - see front matter © 2004 Elsevier B.V. All rights reserved.
doi:10.1016/j.commatsci.2004.07.004

digitized serial sections or through methods like X-ray computed tomography and scanning laser confocal microscopy are not suited for routine engineering applications [1] due to the extensive time and effort involved. Efficient methodologies for generating 3D realizations of material microstructure would enable computation of important engineering properties like electrical conductivity, fluid permeability and elastic moduli using finite element [2,3], discrete medium [1,4] or lattice automata models [5]. For microstructures where the interaction effects between neighboring inclusions have significant impact on the overall behavior of the material, properties must be checked by generating several realizations of the 3D microstructure [6]. Hence, there is a need for alternative procedures that can create numerical realizations of 3D microstructure that closely captures the 3D geometry of real microstructure. Techniques that can use microstructure signatures in real-time to generate 3D realizations can be employed to accelerate prediction of material properties enabling efficient design of materials. An inverse problem of specific interest in this paper is to reconstruct 3D microstructures based on limited statistical descriptors obtained from experimental observations of microstructure on planar sections.

A number of statistical models have been proposed for reconstructing 3D porous media from 2D sections [1,2,6–14]. In such models, statistical descriptors like two-point correlation functions and the lineal path functions of planar images are first measured. Random 3D models are then generated such that they match these statistical properties using optimization procedures like simulated annealing [10,12]. Reconstruction using conditioning and truncation of Gaussian random fields is also a widely used reconstruction technique [2,7,8,11]. Recently Bochenek and Pyrz [6] have applied stochastic reconstruction by applying field quantities like interface stresses as additional constraints in the optimization procedure and obtained good reconstructions. The reconstructed models have been applied to evaluate properties like permeability in [1,12], electrical conductivity in [14], and elastic properties in [2]. Quantitative comparisons of these models with tomographic images have however shown that statistical reconstructions may differ significantly from the original sample in their geometric connectivity [9,11]. Process-based models which account for the physical processes that create the microstructures have been shown to adequately model the geometric connectivity [15]. This additional information can either be obtained through experimental means or through models of microstructure evolution. In this paper, we employ a database of 3D microstructures and perform the reconstruction by posing the underlying inverse problem as a pattern recognition problem instead of an optimization problem. The library of 3D microstructures is generated using Monte-Carlo models of microstructure evolution [16,17] and is used as the data set from which 3D microstructures with matching features are selected. This is achieved through machine learning and classification means using planar image descriptors as features. Following the basic steps of any pattern recognition problem, the corresponding steps for reconstruction of 3D microstructures can be summarized as follows:

- *Database creation:* Several instances of computationally or experimentally obtained 3D microstructures are created and stored within a database.
- *Feature extraction step:* The lower-order features of 3D microstructures based on relevant planar image statistics are extracted.
- *Training step:* Microstructures from the database are arranged into classes having similar lower-order measures. Use of more than one descriptor leads to a class hierarchy. Support vector machines automatically build class partitions based on the extracted features.
- *Prediction step:* Given a planar image, 3D reconstruction of the microstructures are predicted by matching the planar image statistics over a class of 3D microstructures using support vector machines.

An emerging technique called support vector machines (SVM) has been employed for the creation of the class library for three-dimensional microstructures. The method has been adapted for 3D microstructure identification based on prior success of the technique in complex pattern

recognition problems with high dimensional feature sets like handwritten text recognition [18], 3D object identification [19], and texture recognition [20]. SVM is applied for the training and the prediction step of the reconstruction process. Two specific examples of reconstruction of isotropic microstructures through classification means based on a 3D microstructure database are discussed in this paper. In the first case, the full three-dimensional structure of an experimentally obtained 2D polyhedral microstructure of Aluminum alloy (AA3002) [21] has been reconstructed using a grain-size descriptor based on the Heyn intercept technique [22]. The obtained 3D grain size distribution is then compared for validation with stereological predictions [23,24] of 3D grain size distribution. In the second case, we introduce a hierarchical 3D microstructure library based on statistical features of two-phase microstructures for 3D reconstruction. The elastic properties of the reconstructed 3D microstructures have been evaluated using well known variational bounds [25–28] and are compared with experimental results available in the literature [29].

The procedure employed generates a class of 3D microstructures whose lower-order features closely match with the features of a given 2D microstructure. The non-uniqueness of solution is attributed to the use of lower-order features for classification, i.e. several different microstructures might have the same lower-order functions [6,10]. Instead of using several higher-order measures for the mathematical representation of 3D microstructures, a principal component analysis (PCA) technique [30–32] is introduced for enabling reduced-order representation. In this case, classification technique based on lower-order descriptors is shown to increase the efficiency of representation. This technique is shown in an example where full representation of two-phase 3D microstructures has been realized using just two coefficients over a reduced basis within a class of 3D microstructures having similar lower-order measures.

The pattern recognition technique introduced in this paper has applicability to several other problems in materials science where a prior database of information is available and optimum parameters need to be selected. Examples are applications like process design, and parameter selection for optimization of processes or properties based on information available from experiments or physical models. In such situations, the approach predicts solutions in real-time or provides initial guesses to accelerate design in complex multi-objective optimization problems.

The remaining of this paper is arranged into four main sections. Section 2 reviews the general support vector machines classification framework. Sections 3–5 provide relevant examples of applications of microstructure feature classification techniques for reconstruction and reduced representation. The appendix at the end of the paper provides brief overview of the various models employed.

2. Microstructure reconstruction using pattern recognition

A pattern recognition approach works by making decisions on the best realization of a 3D microstructure based on available examples from a database (also called 'the training set'). Many of these decisions are currently performed by human experts, but it is increasingly becoming feasible to design automated systems that can perform such tasks more efficiently. Support vector machine (SVM) is a statistical learning algorithm for pattern classification and regression [33]. The classification involves prior training with features from known 3D microstructure classes. The success of support vector machines is attributed to its underlying statistical learning theory based on structural risk minimization (SRM). The basic idea of support vector machines (SVMs) is to determine a classifier which minimizes the empirical risk (the training set error). Initial description of the support vector machines presented here is restricted to a two-class problem ($p = 2$). Extension to multi-class recognition is described at the end of this section.

Let the n sets of training features (descriptors of 3D microstructure) be given as $(y_i, \mathbf{x}_i)$, $i = 1,\ldots, n$. The training features are from a set of two 3D microstructure classes whose class labels are given as $y \in \{1,-1\}$. Each feature attribute is a vector of

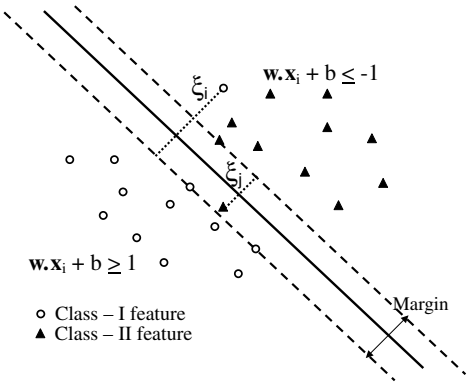

Fig. 1. Support vectors (shown as dotted lines) used for binary classification with feature vectors ($\mathbf{x}_i$) of size $m = 2$: the slack variables (ξ_i and ξ_j) are minimized while maximizing the margin between features from the two classes.

m values as $\mathbf{x}_i^{\mathrm{T}} = \{x_{1i}, \ldots, x_{mi}\}, \mathbf{x}_i \in \Re^m$. The classification problem is then posed as follows:

Statement 1: Given a new planar microstructure with its feature vector defined by $\mathbf{x}^{\mathrm{T}} = \{x_1, x_2, \ldots, x_m\}$, find the class of 3D microstructures ($y \in \{1,-1\}$) to which it is most likely to belong.

The basic form of support vector machines finds the optimal separating plane (Fig. 1) between microstructural features in the m-dimensional space such that the error for unseen test image features is minimized. SVMs can also be used to classify non-separable data by mapping the data to a higher-dimensional feature space where optimal separating planes may be found (Fig. 2).

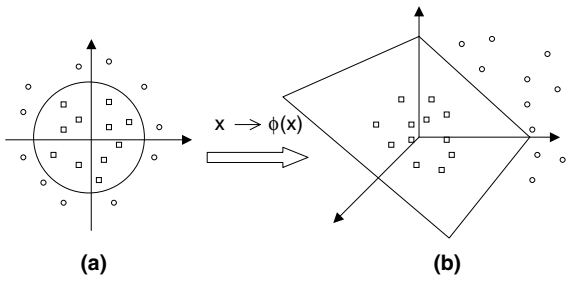

Fig. 2. Mapping data ($\mathbf{x}$) to a higher-dimensional space as $z = \phi(\mathbf{x})$. (a) A linearly non-separable set of microstructural features of dimension $m = 2$. (b) Microstructure features projected to dimension $m = 3$. In this case, an optimal separating hyperplane is found.

2.1. Maximum margin classifier in m-dimensional feature space

The hyperplanes in the m-dimensional space of the feature vectors are of the form $y = \mathbf{w} \cdot \mathbf{x} + b$ where $\mathbf{w}^{\mathrm{T}} = \{w_1, w_2, \ldots, w_m\}$ and b is a scalar. If the data is linearly separable, a decision function $D(\mathbf{x}) = \mathbf{w} \cdot \mathbf{x} + b$ can be determined such that,

$$y_i D(\mathbf{x}_i) \geqslant 1, \quad i = 1, \ldots, n \tag{1}$$

where n is the number of training sets. Since $y \in \{1,-1\}$ (restricting the discussion to two classes, $p = 2$), the decision function is such that $D(\mathbf{x}) \leqslant -1$ when $y_i = -1$, or $D(\mathbf{x}) \geqslant 1$ when $y_i = 1$. Thus, if the hyperplane is placed midway between the two-closest points to the hyperplane, $\mathbf{w}$ and b can be scaled such that $D(\mathbf{x}) = 0$. The distance between the two classes based on this hyperplane is at least $\frac{2}{\|\mathbf{w}\|}$ and is called the margin. The hyperplane with the highest margin (minimum $\|\mathbf{w}\|$) is called the optimal hyperplane. Hence, the problem of finding the optimal hyperplane reduces to the optimization problem of minimizing the cost functional,

$$J(\mathbf{w}) = \frac{1}{2}\|\mathbf{w}\|^2 \tag{2}$$

given the n inequality constraints of Eq. (1). This optimization problem can be solved in several ways, but the most efficient solution scheme is to pose it as a quadratic programming problem.

2.2. Non-linear classifier

For data that cannot be linearly separated in the m-dimensional space of the feature vector (Fig. 2(a)), support vector machines non-linearly maps the data $\mathbf{x}$ to a higher-dimensional feature space (Fig. 2(b)) as $z = \phi(\mathbf{x})$ where an optimal hyperplane is found. A positive definite kernel is defined as $K(\mathbf{x}_1, \mathbf{x}_2)$, specifying an inner product in the feature space, $K(\mathbf{x}_1, \mathbf{x}_2) = \phi(\mathbf{x}_1) \cdot \phi(\mathbf{x}_2)$. The solution for the optimization problem (Eq. (2)) is then given by $\mathbf{w} = \sum_{i=1}^{n} \alpha_i y_i \phi(\mathbf{x}_i)$ for $\alpha_i \geqslant 0$. The problem of determining the α_i's is once again posed as a quadratic programming problem of maximizing [33],

$$W(\alpha) = \sum_{i=1}^{n} \alpha_i - \frac{1}{2} \sum_{i,j=1}^{n} y_i y_j \alpha_i \alpha_j K(\mathbf{x}_i, \mathbf{x}_j) \tag{3}$$

in the positive quadrant $\alpha_i \geqslant 0$, $i = 1,\ldots,n$, subject to the constraint, $\sum_{i=1}^{n} \alpha_i y_i = 0$. Optimal b is then found as $b = y_i - \boldsymbol{w} \cdot \mathbf{x}_i$, where $i = \arg\ \max_k(\alpha_k)$. The support vectors are the points for which $\alpha_i > 0$ satisfying Eq. (1) with equality. When the data is non-separable in the higher-dimensional feature space, slack variables $\xi_i \geqslant 0$ are introduced such that $y_i D(\mathbf{x}_i) \geqslant 1 - \xi_i$, $i = 1,\ldots,n$ to allow the possibility of samples to violate Eq. (1). Fig. 1 shows the optimal hyperplane with the slack variables (ξ_i) indicated. The idea is to maximize the margin and minimize the training error (represented by the slack variables) simultaneously. The cost function (Eq. (2)) to be minimized is modified as,

$$J(\mathbf{w}, \xi) = \frac{1}{2}\|\mathbf{w}\|^2 + C \sum_{i=1}^{n} \xi_i \tag{4}$$

where the purpose of C in the second term is to control the number of misclassified points.

2.3. Prediction of classes using support vectors

Prediction step of the pattern recognition problem provides solution to Statement 1. The training step of the support vector machine creates a hyperplane of the form $\mathbf{w} \cdot \phi(\mathbf{x}) + b = 0$ such that the features from class 1 lie on the positive side of the hyperplane and features from class 2 lie on the negative side. Hence, given a new microstructural feature $\mathbf{x}^{\mathrm{T}} = \{x_1, x_2, \ldots, x_m\}$, the sign of the expression $\mathbf{w} \cdot \phi(\mathbf{x}) + b$ (the 'decision function', $f(x) \in \{-1,1\}$) gives the 3D microstructure class ($y \in \{1,-1\}$) to which the image is most likely to belong. The decision function can be written as follows:

$$f(\mathbf{x}) = \operatorname{sgn}\left(\sum_{i=1}^{n} \alpha_i y_i K(\mathbf{x}_i, \mathbf{x}) + b \right). \tag{5}$$

Microstructure classification is inherently a multi-class problem (or a multi-objective optimization problem) with several microstructural features of different dimensions that need to be mapped over several classes of microstructure. Hence, the problem statement for microstructure reconstruction needs to be modified as,

Statement 2: Given a new planar microstructure with its s features given by $\mathbf{x}_1^{\mathrm{T}} = \{x_1^1, x_2^1, \ldots, x_{m_1}^1\}, \mathbf{x}_2^{\mathrm{T}} = \{x_1^2, x_2^2, \ldots, x_{m_2}^2\}, \ldots, \mathbf{x}_s^{\mathrm{T}} = \{x_1^s, x_2^s, \ldots, x_{m_s}^s\}$, find the class of 3D microstructure ($y \in \{1,2,3,\ldots, p\}$) to which it is most likely to belong.

Following the analysis over two classes, extending the method for classifying microstructures to p classes ($p > 2$) is straightforward. SVM in general is very effective for the case when two classes ($y \in \{1,-1\}$) exist. To extend the scope of SVM to multi-class problems one has to construct $p(p-1)/2$ classifiers where each classifier is trained on data from two classes. This method called the 'one-against-one' method [34] has been employed for the microstructure classification problem. If between two classes i and j, a given data set is classified to class i, then the vote for class i is incremented by one. Given a data point, $p(p-1)/2$ classifications are performed and the data is classified to the class which gets the maximum votes. In case of a tie, the microstructure class with a smaller index is selected.

For matching over multiple features ($s > 1$), we employ a hierarchical classification structure. An example for the hierarchical structure for two-phase 3D microstructure is shown in Fig. 3. The features ($s = 2$) are the autocorrelation and the three-point probability functions (refer to Section 4.1). Once the 3D microstructure class 'i' matching the first feature ($\mathbf{x}_1$: the autocorrelation function) is identified, the classifier moves on to the next level and classifies images from within class 'i' based on the second feature ($\mathbf{x}_2$: the three-point probability function). The analysis can be extended to several levels for creating realizations of 3D microstructures having multiple features similar to the reference planar microstructure. SVMs are currently the best pattern recognition systems for several difficult multi-class problems like hand-written character recognition and provide computationally efficient alternative to direct optimization. Advantages of SVM for microstructure classification problems have been further highlighted in this paper by comparing the technique with traditional methods like probabilistic

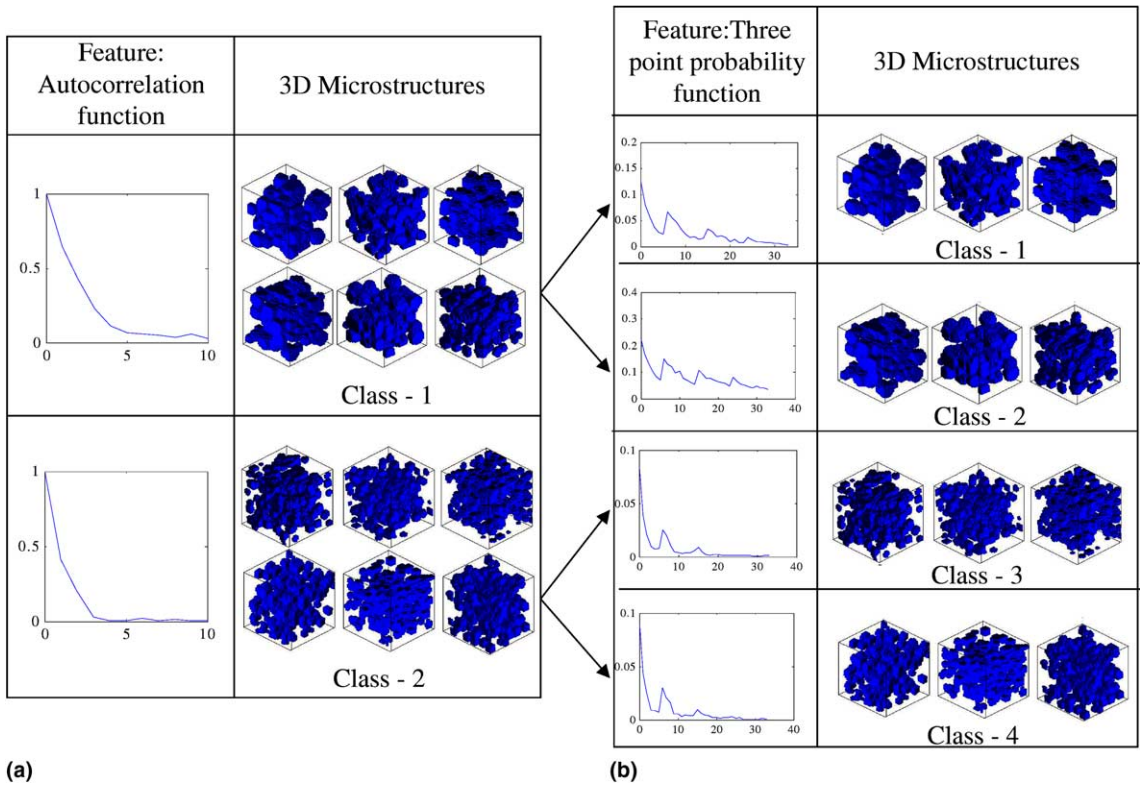

Fig. 3. Hierarchical multi-class classification. (a) Level 1: 3D microstructure classes based on autocorrelation function. (b) Level 2: sub-classes based on three-point probability function.

neural networks, linear discriminant classifier and decision trees (see Section 3). Further, reconstruction and subsequent analysis of the reconstructed microstructures have been performed for polyhedral and two-phase microstructures.

3. Example 1. 3D reconstruction of polyhedral microstructures

Several important engineering materials consist of grains with convex polyhedral shapes filling the microstructure. The shape and distribution of grain boundaries over such microstructures have influences on material transport properties like thermal and electrical conductivity. Stochastic models based on methods like random spatial tessellations or Monte-Carlo grain growth simulations provide 3D representation of such microstructures. Selection of appropriate 3D microstructure models based on available planar images would enable analysis of properties in 3D geometries through finite element analysis [3] or discrete medium models [4]. Using support vector machine classification, we present a method of selection of three-dimensional microstructures corresponding to a planar polyhedral microstructure image using a geometrical size feature based on planar sections of the 3D image. The grain size distribution of the 3D reconstructed class is then compared with stereological estimates for validation.

3.1. Classification of polyhedral microstructures

Reconstruction methods for planar images depend on the assumption of randomness, i.e. the microstructure is assumed as homogeneous and isotropic. This assumption of randomness is called

the model-based approach [24, p. 165] wherein grains are assumed to have a constant shape but varying size. Information about the 3D structure can then be realized using information from arbitrarily chosen planar sections of microstructure. Fig. 4 shows a 2D image that was employed as an example for 3D reconstruction. The image is a polarized light micrograph of a commercial aluminium alloy (AA3002) obtained from the literature [21]. The grain size feature based on the image is obtained using the Heyn intercept technique [22].

In the Heyn's intercept method, a network of parallel equidistant lines of known length are placed over the microstructure image over several orientations and the number of grain boundary intersections with each test line is measured. Histograms of the intercept length distribution (mean intercept length versus number of test lines possessing the mean intercept length) are used as a feature parameter for the grain size distribution. Consistent features were extracted from planar sections of the 3D microstructure and the use of lineal intercepts at several angles over the planar samples to even out effects of anisotropy. The mean intercept histogram is subsequently used as the training set in the classifier. The database containing 120 3D images was classified into six classes with 20 images each and n-fold cross-validation tests were performed to test the accuracy of feature set. In an n-fold cross-validation, the training set is randomly divided into n subsets of equal size. Sequentially one subset is tested using the classifier trained on the remaining $n-1$ subsets. The class of every instance of the whole training set is predicted once, hence, the cross-validation accuracy is the percentage of data that are correctly classified. A linear SVM was employed for the study and the efficiency of SVM has been brought out by comparing its efficiency with MATLAB® implementations of probabilistic neural network, linear discriminant classifier, and decision tree classification models. A comparison of average cross validation accuracy of all the techniques is listed in Table 1.

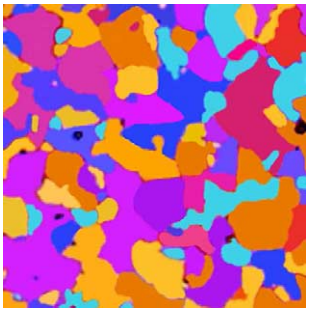

Fig. 4. A polarized light micrograph of Aluminum alloy AA3002 representing the rolling plane [21] ($600 \times 600\,\mu m^2$).

The images used in the library represent 3D microstructures obtained computationally using a Monte-Carlo Potts grain growth model (refer to Appendix C.1). The dimensions of the 3D microstructures in the library are $128 \times 128 \times 128\,\mu m^3$. The size feature of the experimental 2D image is appropriately scaled to match this dimension before providing it to the pattern recognition system. The reconstructed 3D microstructures are then rescaled to match the 2D image size. A representative microstructure of the 3D class reconstruction of the 2D experimental image (Fig. 4) is shown in Fig. 5. A comparison of the average grain size feature of the reconstructed 3D image class and the size feature of the 2D experimental image is shown in Fig. 6. The accuracy of the pattern

Table 1
Comparison of SVM and traditional techniques using n-fold cross validation (CV) test on the lineal intercept feature measure

CV set(n)	Neural net	Linear discriminant	Decision trees	SVM
10	81.6712	81.3924	81.1538	85.9504
6	81.4676	81.4738	80.7619	85.9504
5	81.1117	80.5657	80.4010	85.1240
4	80.7010	80.9036	79.9032	84.2975
3	78.9123	80.2818	79.0244	84.7769

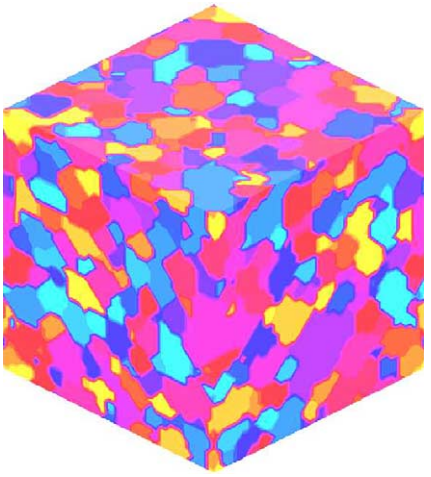

Fig. 5. A representative image from the reconstructed class of image in Fig. 4 (edge length = 600 μm).

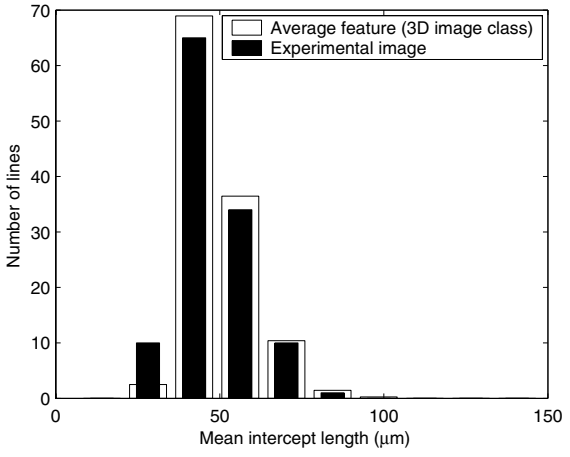

Fig. 6. Comparison of the two-dimensional grain size feature and the average feature of the three-dimensional class of microstructures.

recognition technique is demonstrated by the high feature correlation ($R^2 = 98.7946\%$) achieved.

In order to further test the applicability of the 3D microstructure selection technique, we carry out a stereological analysis of the planar image. The method has been employed for estimating the expected size distribution for a 3D image using the grain sizes in the 2D image. The grain size distribution of the reconstructed 3D microstructure is then compared with the predicted 3D size distribution to test the reconstruction.

The estimation of 3D grain size distribution from grain size data sampled from planar images is called the 'stereological unfolding problem' [24]. Let U be a random grain size in a 3D microstructure. Similarly, let S be a random grain size in the sectional profile where the size is defined as the maximum caliper diameter of a grain. The stereological problem involves estimation of the density of grains (mean number/volume, N_v) and the size-distribution probabilities ($F_v(u)$) over a volume from the density (N_a) and the size-distribution ($F_a(s)$) of grains observed in a planar section. The general stereological problem can be given by [24, p. 201],

$$\frac{N_a(1-F_a(s))}{N_v} = \bar{b}\int_0^\infty u[1-G_u(s)]dF_v(u), s \geqslant 0, \tag{6}$$

where $\bar{b}$ is the rotation average of the size of a particle with maximum caliper diameter of one and $G_u(s)$ is a conditional size-distribution function of grains in the planar section. The kernel function $p(u,s) = \bar{b}u[1-G_u(s)]$ depends on the shape assumption of the grains in the microstructure. The discrete version of the stereological equation can then be written as,

$$N_a(1-F_a(s)) = \sum_{i=-\infty}^{\infty} p(u_i,s)v_i, \tag{7}$$

where v_i is the mean number per unit volume of grains with size u_i. By discretizing the size distribution in terms of logarithm of sizes in equally spaced bins (where $u_i = a^i$ and $s_k = a^k$ with discretization parameter $a = \sqrt{2}$) [24], a linear equation system of the form $y = P\theta$ is obtained which can be solved for the 3D size-distribution. Here, y_k is the mean number per unit area of the section profiles with sizes between s_{k-1} and s_k such that $y_k = N_a[F_a(s_k) - F_a(s_{k-1})]$, $\theta_i = \bar{b}a^i v_i$ and P is a matrix corresponding to the discretized kernel function that depends on the assumed shape of grains in the microstructure.

The coefficients in P for the case when the particles shapes are approximated to be randomly sized and oriented cubes are presented in

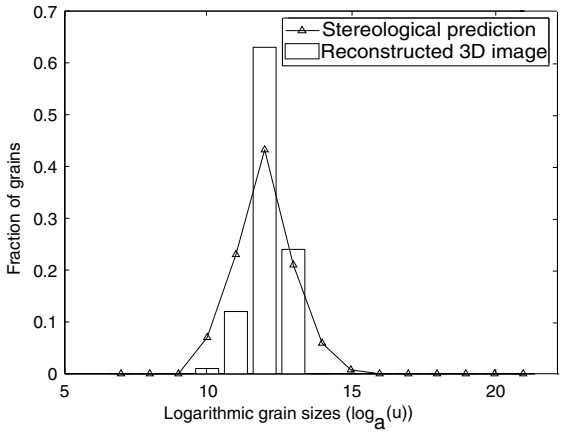

Fig. 7. Comparison of the 3D size-distribution of a representative image in the 3D class and corresponding stereological estimates obtained using the image in Fig. 4.

[24, p. 205]. In a related study [23], the cube distribution was found to estimate the spatial grain size distribution better than spherical or polyhedron models of grains. The classification results for the grain size distribution in 3D as compared with the stereological estimates are presented in Fig. 7. The stereological estimate of 3D grain size-distribution agrees qualitatively with the grain size distribution in the reconstructed 3D microstructure with correlation $R^2 = 80.5798\%$. The peaks of the expected distribution are well captured by the reconstructed microstructure. The reconstructed grain size distributions were compared with the estimates obtained for several cases of microstructures tested and were found to have good agreement, bringing out the efficiency of the feature classification approach.

4. Example 2. 3D reconstruction of two-phase microstructures

Statistical three-dimensional reconstruction of two-phase microstructures is a problem extensively studied in the literature [1,2,6–14]. The method employs the statistical information available in a planar microstructure image to construct the 3D representation. With the availability of computational modeling tools and 3D imaging methods,

Fig. 8. Experimental Tungsten-silver composite image ($204 \times 236\,\mu m$) from Umekawa et al. [29].

a 3D microstructure library approach based on pattern recognition is a promising approach for producing 3D representations of microstructures using relevant 2D image statistics. In this section, we outline a method for matching multiple statistics of planar images based on a hierarchical classification framework. The experimental data in Ref. [29] provides a high resolution planar microstructure image (Fig. 8) that has been employed for several reconstruction studies [2,35]. For the purposes of generating realistic porous structures of Tungsten, a Monte-Carlo technique [17] (refer to Appendix C.2) has been employed. Several 3D configurations were obtained, and statistical features extracted from these 3D microstructures were employed for developing the microstructure classes in the library.

4.1. Feature extraction—statistical correlation functions

For the reconstruction of the planar two phase microstructure image and also for the calculation of the property bounds, rotationally invariant probability functions are employed as the microstructural features, assuming isotropic nature of the microstructure. As indicated in [36,37], reconstructing the probability functions only in certain directions with the isotropy assumption may artificially introduce a strong anisotropy or affect the connectivity. Rotationally invariant N-point correlation measure (S_N^i) can be interpreted as the probability of finding the N vertices of a polyhedron separated by relative distances $x_1, x_2, \ldots, x_N$

in phase i when tossed, without regard to orientation, in the microstructure. The simplest of these probability functions is the one-point function, S_1^i, which is just the volume fraction (V) of phase i. The two-point correlation measure, $S_2^i(r)$, can be obtained by randomly placing line segments of length r within the microstructure and counting the fraction of times the end points fall in phase i. These statistical descriptors occur in rigorous expressions for the effective electromagnetic, mechanical, and transport properties like effective conductivity, magnetic permeability, effective elastic modulus, Poisson's ratio, and fluid permeability of such microstructures (consult the reviews in Refs. [28,35]). Property bounds on the elastic modulus and Poisson's ratio of two-phase systems reported in the literature are, (a) the Hashin–Shtrikman (HS) bound [27] which implicitly depends on the two-point correlation measure and (b) the Beran–Molyneux–Milton–Phan–Thein (BMMP) bound [26,25], which is based on three-point statistical correlation measure of the microstructure. Through the use of higher-order correlation functions, further restrictions can be applied on the property bounds on the microstructure.

All the required correlation measures for classification and property bound calculation are obtained using a Monte-Carlo sampling procedure [38]. The procedure involves initially selecting a large number of initial points in the microstructure. For every initial point, several end points at various distances are randomly sampled and the number of successes (of all points falling in the ith phase) are counted to obtain the required correlation measures. Statistical measures up to the third-order were extracted from the microstructures by sampling 15,000 initial points and are used as feature vectors for classifying the 3D images in the library.

4.2. 3D image reconstruction from 2D section

A 657×657 pixel region of the microstructure corresponding to 204 μm square area was converted to a black and white image for distinguishing the two phases. The rotationally invariant two- and three-point correlation measures of the experimental image were then extracted using Monte-Carlo sampling techniques.

Initially a set of 120 3D microstructure images were generated and stored in the library. Classification is based on two sets of descriptors, the autocorrelation function $\gamma(r) = \frac{S_2(r)-p^2}{p-p^2}$ and the three-point measure $S_3(r,s,t)$. A two-step hierarchy is introduced wherein an initial cluster of microstructures containing comparable autocorrelation measures are further classified based on the three-point measure (Fig. 3). Matching the features of the planar image over the library using support vector machines results in a class of 3D microstructures having statistical measures similar to the experimental image. The reconstruction took 0.5610 s on a 930 MHz x-86 P-3 Intel processor. An instance of the reconstructed microstructure is shown in Fig. 10. The statistical correlation measures of the reconstructed 3D microstructure and the experimental image are compared in Fig. 9. The three-point probability measure $S_3(r,s,t)$ is depicted in a feature vector format with the distances (r,s,t) μm indicated for key points in Fig. 9(b). The variational bounds on the elastic modulus of the reconstructed representative 3D microstructure are then calculated and compared with experimental results in Fig. 11. The results are based on the measured elastic moduli of each phase (corrected for the porosity effects) as presented in [2]. The microstructure parameters ξ and η (refer to Appendix B) of the reconstructed microstructure as found by evaluating the Eqs. (B.3) and (B.4) are 0.223 and 0.368, respectively. The BMMP upper bounds on the elastic modulus of the reconstructed 3D microstructure closely follows the experimental microstructure properties. Further, exact elastic moduli of the reconstructed 3D microstructure were calculated using finite element analysis. The method operates on a 3D image through a pixel-based mesh and for a given microstructure, subject to an external strain, the final elastic displacement distribution is obtained such that the total energy stored is minimized, or the gradient of the elastic energy with respect to the displacement is zero. Further details of the method employed and the software used in this implementation are given in [39]. The computed properties closely follow the BMMP upper bounds and the experimental Young's

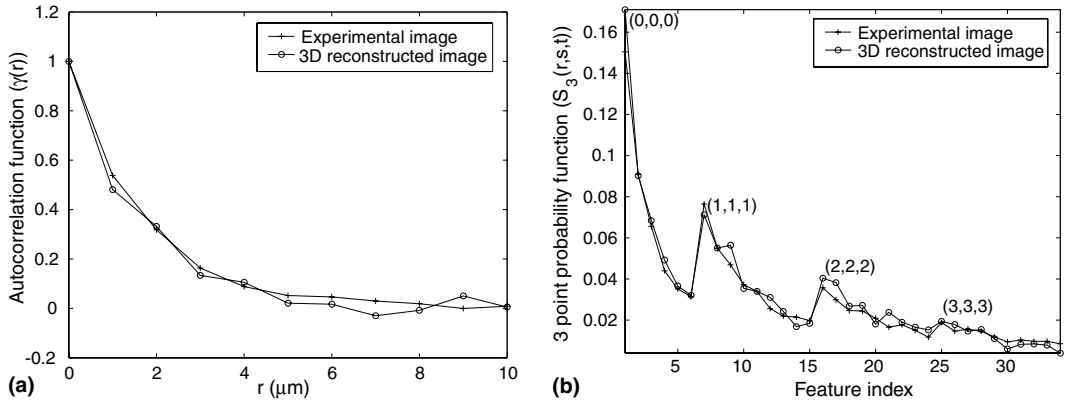

Fig. 9. Comparison of the experimental image statistical features with the features of the reconstructed image shown in Fig. 10. (a) The autocorrelation function and (b) the three-point probability function $S_3(r,s,t)$ shown in a feature-vector form with select (r,s,t) indicated.

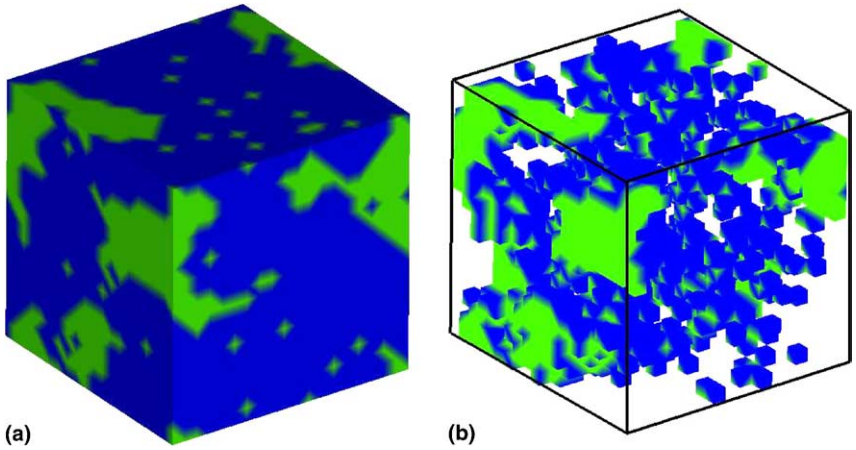

Fig. 10. (a) A $20\,\mu m \times 20\,\mu m$ space of reconstructed 3D microstructure of the experimental image and (b) the silver phase of the reconstructed microstructure.

modulus. Thus, using the pattern recognition approach, realistic 3D microstructures that efficiently capture the microstructure–property relationships of the reference image are obtained.

5. Reduced-order representation of 3D microstructures

Reconstruction based on the image library approach yields several possible spatial realizations (a class of 3D microstructures) for a given planar image when lower-order features are employed for classification. This is attributed to the absence of complete morphological information in such lower-order measures [10] resulting in non-uniqueness, i.e. several different microstructures having the same lower-order measures. Hence, lower-order measures cannot alone be used for completely characterizing microstructures. However, lower-order features can be efficiently employed for mathematical representation of microstructures by following a classification-based approach. This is accomplished in two steps. Firstly, 3D

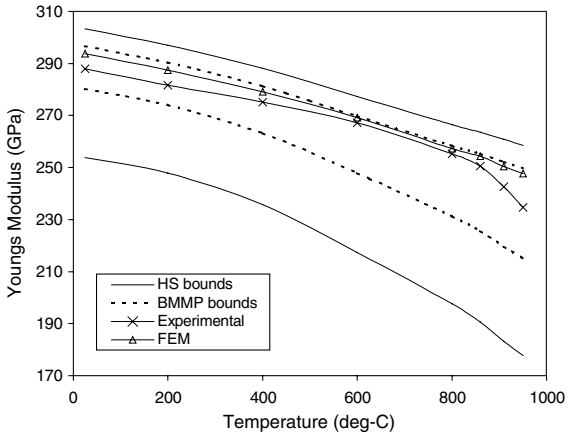

Fig. 11. Experimental Young's modulus is shown along with the computed HS and BMMP bounds for the reconstructed 3D microstructure. A numerical (FEM) result for the Youngs Modulus of the reconstructed microstructure is also indicated.

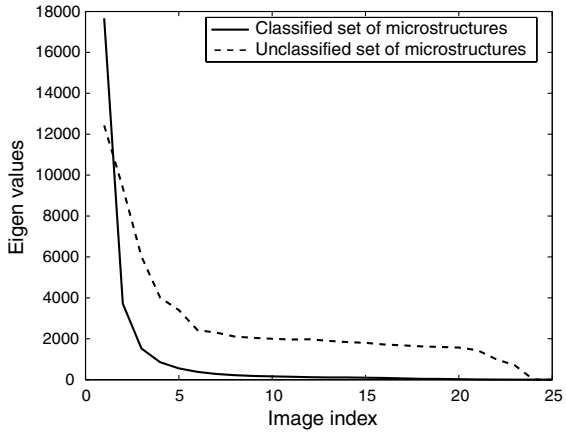

Fig. 12. The spectrum of eigenvalues obtained by PCA decomposition of a classified 3D microstructure set (continuous line) and an unclassified set (dotted line). For the unclassified case, the eigenvalues do not decay to zero. Hence, the entire eigenbasis needs to be used for representation.

images are classified based on lower-order features like grain sizes, shapes and point probability measures into several user-trained classes using support vector machines. Following this, principal component analysis [30–32] (refer to Appendix A) is employed for the mathematical representation of the microstructures. The highlights of the method are presented using an example in this section.

5.1. Reduced-order representation example: two-phase microstructure

A class of 25 3D microstructures with similar two-point descriptors obtained from a Monte-Carlo simulation of two-phase solidification was employed for this study. Principal component analysis over the class yields a microstructure basis over which images can be represented as coefficients (Appendix A). The spectrum of eigenvalues for the classified set of microstructures is shown in Fig. 12. Eigenvalues decay rapidly and the information in the first few eigenvalues captures the essential features of the microstructure, and hence images can be effectively represented by a small fraction of the eigenbasis. The rapid decay of the eigenvalues is attributed to prior classification which ensures that the microstructures are similar in structure. This feature of classification is brought out by comparing the eigenvalues arising from the classified structures and an unclassified set of microstructures in Fig. 12. The eigenvalues do not decay to zero for the unclassified set and hence, the entire eigenbasis needs to be employed for 3D microstructure representation. This increases the number of representation coefficients required for microstructure representation over large databases. Classification provides a natural way of reducing the number of representation coefficients required, since the majority of the eigenvalues are mostly zeroes as seen in Fig. 12.

The eigenvectors corresponding to the largest eigenvalues for the classified set of 3D microstructures are shown in Fig. 13. Any 3D microstructure within the class is a linear combination of these eigenmicrostructures and the coefficients of the linear combination provides the numerical representation for the 3D microstructure. As an example, the microstructure in Fig. 14(a) was represented as a linear combination of the first two eigenvectors which yields two coefficients for the microstructure. Reconstruction of the 3D image using these coefficients resulted in the microstructure shown in Fig. 14(b). The two-phase microstructure was represented in binary, with '1' depicting the

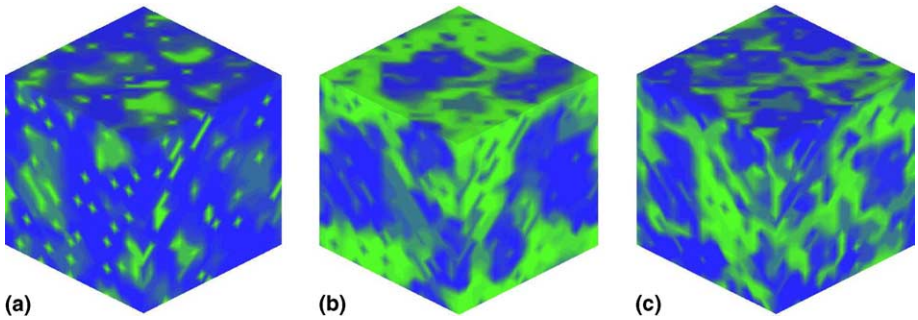

Fig. 13. Eigenmicrostructures in the decreasing order of eigenvalues λ (a) $\lambda = 1.7666e4$, (b) $\lambda = 0.3719e4$, (c) $\lambda = 0.1522e4$.

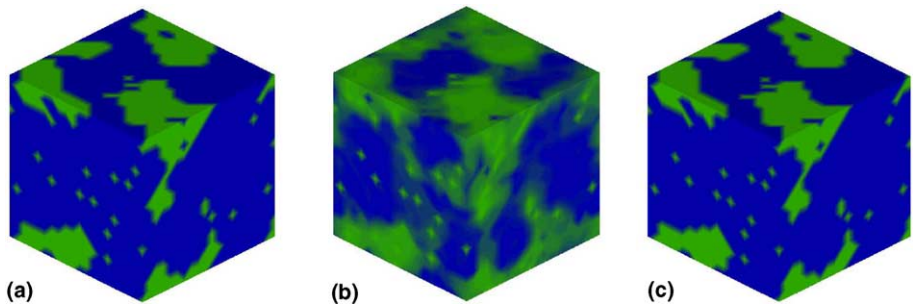

Fig. 14. (a) The test microstructure to be reconstructured, (b) reconstruction based on first two eigenvalues, the corresponding representation coefficients are (5.8951,14.8675) and (c) reconstructed microstructure after rounding off fractional pixel values.

porous solid structure and '0' representing the surrounding matrix. The microstructure reconstructed using two eigenvectors contained fractional values due to the removal of smaller basis components. When the fractional pixel values were rounded off, the resulting image shown in Fig. 14(c) becomes exactly the same as the original microstructure in Fig. 14(a). The classification-PCA framework has hence enabled reduced-order representation of the 3D microstructure with just two coefficients. The first few eigenmicrostructures over which the images are represented form the central component of a dynamic library of microstructures that can be used for microstructure quantification. An improved technique called incremental principal component analysis that works in conjunction with SVM classification and updates the representation in real-time has been recently proposed by the authors [32].

6. Conclusions

A 3D microstructure classification framework has been developed based on support vector machines, an efficient statistical learning technique. Applications of pattern recognition over a microstructure database are shown using examples of 3D reconstruction of planar images. Support vector machines produces a class of microstructures with features close to the reference microstructure. The reconstruction algorithm efficiently matches multiple features through a hierarchical classification scheme. Viability of the method has been illustrated by comparing the features of the reconstructed microstructures on the basis of stereological predictions and microstructure–property relationships. Further, classification using lower-order descriptors has been shown to improve the quantification of microstructures. Principal component analysis

over a classification structure is suggested as an efficient method for reduced-order representation of microstructures.

A machine learning approach provides an attractive and computationally viable solution to the 3D representation of complex microstructures given limited information over a planar section. Further, research on statistical learning methods for applications like process sequence selection and selection of appropriate processing parameters that lead to desired microstructures and tailored properties are currently underway. The parameters produced by such approaches have been used as efficient initial guesses that are fine-tuned by computational models within an optimization framework (preliminary results were presented in [40]). The machine learning approaches thus synergistically interact with physically based models, accelerating the design and improvement of materials.

Acknowledgments

The work presented here was funded by the Mechanical Behavior of Materials program (Dr. D. Stepp, program manager) of the Army Research Office (proposal No. 45850-MS) and by the Computational Mathematics program (Dr. F. Fahroo, program manager) of the Air Force Office of Scientific Research (grant FA9550-04-1-0070). This research was conducted using the resources of the Cornell Theory Center, which receives funding from Cornell University, New York State, federal agencies, and corporate partners.

Appendix A. Principal component analysis

Using a set of large-dimensional data called the 'snapshots', this method decomposes the data into an optimal orthonormal basis [30,32]. Let N different 3D microstructure images (I_i), each of size n pixels by n pixels by n pixels are to be represented. The images are converted into N vectors ($\mathbf{X}^{(i)}$) and the average is computed as $\mu = \frac{1}{N}\sum_{i=1}^{N}\mathbf{X}^{(i)}$. The average image ($\mu$) is then subtracted from all the image vectors as $\mathbf{X}^{(i)} \leftarrow \mathbf{X}^{(i)} - \mu$, for $i = 1,\ldots,N$. The eigenvectors $\mathbf{U}^{(k)}$ of the $n^3 \times n^3$ covariance matrix $C = \frac{1}{N}\sum_{i=1}^{N}\mathbf{X}^{(i)}\mathbf{X}^{(i)^{\mathrm{T}}}$ satisfying

$$\mathbf{C}\mathbf{U}^{(k)} = \lambda_k \mathbf{U}^{(k)}, \quad k = 1,\ldots,n^3 \tag{A.1}$$

with the eigenvalues λ form the best basis for the images. Even though the above method calculates the best uncorrelated basis, it is computationally intensive. An efficient approach is the so called 'method of snapshots'. Here, the property that the eigenvectors $\mathbf{U}^{(k)}$ are the unique linear combinations of the microstructure images ($\mathbf{X}^{(i)}$) are exploited and can thus be written as

$$\mathbf{U}^{(k)} = \sum_{j=1}^{N} \alpha_{jk}\mathbf{X}^{(j)}, \quad k = 1,\ldots,N \tag{A.2}$$

Let us define $\mathbf{C}^*$ as $\mathbf{X}^{(i)^{\mathrm{T}}}\mathbf{X}^{(j)}$, $i, j = 1,\ldots,N$, and let the vector $\mathbf{E}^{(k)} = \alpha_{ik}$, $i = 1, \ldots,N$, denote the coefficients of the eigenvector $\mathbf{U}^{(k)}$ in the basis of the snapshots. Then the original eigenvalue problem Eq. (A.1) is equivalent to the following eigenvalue problem,

$$\mathbf{C}^*\mathbf{E}^{(k)} = \lambda_k^*\mathbf{E}^{(k)} \tag{A.3}$$

A $N \times N$ matrix, $\mathbf{X}^{(i)^{\mathrm{T}}}\mathbf{X}^{(j)}$ is constructed and the vectors $\mathbf{E}^{(k)}$, $k = 1,\ldots,N$ are found from the solution of the above eigenvalue problem. The N eigenvectors $\mathbf{U}^{(k)}$ are subsequently found using Eq. (A.2). These vectors form the so called 'eigenmicrostructures', $\mathbf{U}$, which are subsequently normalized. Once the eigenbasis for the set of microstructures in the class is identified, any new image corresponding to that class can be represented by transforming the image into the eigenmicrostructure components by a projection operation. The coefficients (ω_k) of the new image (Γ) in the normalized eigenbasis are given by

$$\omega_k = \mathbf{U}^{(k)^{\mathrm{T}}}(\Gamma - \mu) \tag{A.4}$$

The coefficients (ω_k) form a vector $\Omega = [\omega_1,\ldots,\omega_N]^{\mathrm{T}}$ that is used as a reduced-order representation for the image. The matrix of coefficients of the input images $[\Omega_1,\ldots,\Omega_N]$ is denoted by $\mathbf{A}$, the representation matrix.

Appendix B. Elastic property bounds

Bounds have been derived for properties like conductivity and elastic moduli of composite

materials (a comprehensive review is provided in Ref. [41]). The property bounds for the bulk modulus κ_e and the shear modulus μ_e for well-ordered materials with phase-1 (of volume fraction p) and phase-2 (of volume fraction q (=1 − p)) take the general form [28]:

$$\left(\langle\kappa^{-1}\rangle - \frac{4pq(\kappa_2^{-1}-\kappa_1^{-1})^2}{4\widetilde{\langle\kappa^{-1}\rangle}+3\Gamma}\right)^{-1} \leqslant \kappa_e \leqslant \left(\langle\kappa\rangle - \frac{3pq(\kappa_2-\kappa_1)^2}{3\widetilde{\langle\kappa\rangle}+4\Lambda}\right) \tag{B.1}$$

$$\left(\langle\mu^{-1}\rangle - \frac{pq(\mu_2^{-1}-\mu_1^{-1})^2}{\widetilde{\langle\mu^{-1}\rangle}+6\Xi}\right)^{-1} \leqslant \mu_e \leqslant \left(\langle\mu\rangle - \frac{6pq(\mu_2-\mu_1)^2}{6\widetilde{\langle\mu\rangle}+\Theta}\right) \tag{B.2}$$

where κ_1,κ_2 are the bulk moduli of phase 1 and phase 2, respectively and μ_1,μ_2 are the corresponding shear moduli with $\mu_2 \geqslant \mu_1$ and $\kappa_2 \geqslant \kappa_1$. Here, $\langle x\rangle = px_1 + qx_2$, $\langle\tilde{x}\rangle = qx_1 + px_2$ and the parameters Γ,Θ,Λ,Ξ depend on the microstructural information. If only the volume fractions of the composite are known, $\Gamma = \mu_1^{-1}$, $\Lambda = \mu_2$, $\Xi = \frac{\kappa_1+2\mu_1}{\mu_1(9\kappa_1+8\mu_1)}$ and $\Theta = \frac{\mu_2(9\kappa_2+8\mu_2)}{\kappa_2+2\mu_2}$. The above bound is called the Hashin–Shtrikman bound [27].

If further information is available in terms of statistical two-point $S_2(r)$ and three-point $S_3(r,s,t)$ probability functions, it is possible to further restrict the bounds using the variables ξ_1 and η_1 given by,

$$\xi_1 = \frac{9}{2pq}\int_0^\infty \frac{\mathrm{d}r}{r}\int_0^\infty \frac{\mathrm{d}s}{s} \times \int_{-1}^{1} P_2(u)\left(S_3(r,s,t) - \frac{S_2(r)S_2(s)}{p}\right)\mathrm{d}u \tag{B.3}$$

$$\eta_1 = \frac{5}{21}\xi_1 + \frac{150}{7pq}\int_0^\infty \frac{\mathrm{d}r}{r}\int_0^\infty \frac{\mathrm{d}s}{s} \times \int_{-1}^{1} P_4(u)\left(S_3(r,s,t) - \frac{S_2(r)S_2(s)}{p}\right)\mathrm{d}u \tag{B.4}$$

where $t^2 = r^2 + s^2 - 2rsu$, $P_2(u) = \frac{1}{2}(3u^2-1)$ and $P_4(u) = \frac{1}{8}(35u^4 - 30u^2 + 3)$ are Legendre polynomials.

Using ξ_1 and η_1, the parameters Γ, Λ, Ξ, Θ in Eqs. (B.1) and (B.2) can be expressed as,

$$\Gamma = \langle\mu^{-1}\rangle_\xi, \tag{B.5}$$

$$\Lambda = \langle\mu\rangle_\xi, \tag{B.6}$$

$$\Xi = \frac{5\langle\mu^{-1}\rangle_\xi\langle 6\kappa^{-1}-\mu^{-1}\rangle_\xi}{\langle 128\kappa^{-1}+99\mu^{-1}\rangle_\xi + 45\langle\mu^{-1}\rangle_\eta} + \frac{\langle\mu^{-1}\rangle_\eta\langle 2\kappa^{-1}+21\mu^{-1}\rangle_\xi}{\langle 128\kappa^{-1}+99\mu^{-1}\rangle_\xi + 45\langle\mu^{-1}\rangle_\eta}, \tag{B.7}$$

$$\Theta = \frac{3\langle\mu\rangle_\eta\langle 6\kappa+7\mu\rangle_\xi - 5\langle\mu\rangle_\xi^2}{\langle 2\kappa-\mu\rangle_\xi + 5\langle\mu\rangle_\eta} \tag{B.8}$$

with, $\langle b\rangle_\xi = \xi_1 b_1 + (1-\xi_1)b_2$ and $\langle b\rangle_\eta = \eta_1 b_1 + (1-\eta_1)b_2$.

The new statistical bound obtained by using these values of Γ, Λ, Ξ, Θ in Eqs. (B.1) and (B.2) is called the Beran–Molyneux–Milton–Phan–Thein (BMMP) bound [25,26].

Once the bounds on κ and μ are found, the Youngs Modulus E and Poisson's ratio υ for the material can be bounded as,

$$\frac{9\kappa_l\mu_l}{3\kappa_l+\mu_l} \leqslant E \leqslant \frac{9\kappa_u\mu_u}{3\kappa_u+\mu_u} \tag{B.9}$$

$$\frac{3\kappa_l-2\mu_u}{6\kappa_l+2\mu_u} \leqslant \upsilon \leqslant \frac{3\kappa_u-2\mu_l}{6\kappa_u+2\mu_l} \tag{B.10}$$

where the subscripts l and u refer to the lower and upper bounds defined in Eqs. (B.1) and (B.2).

Appendix C. Monte-Carlo technique

C.1. Polyhedral microstructure

3D polycrystalline microstructures were generated using the Monte-Carlo simulation procedure using a Potts model simulating curvature driven grain growth. In this method, the polycrystal is mapped to a 3D lattice with N_s lattice sites. A grain orientation, s_i, $1 \leqslant s_i \leqslant N_d$ is randomly assigned to each lattice site with index i. The Potts

Hamiltonian, H is used to change grain orientations,

$$H = J\sum_{i=1}^{N_s}\sum_{j=1}^{N_n(i)}(1-\delta_{s_i s_j}) \tag{C.1}$$

where $N_n(i)$ is the number of nearest neighbors of the ith site and $\delta_{s_i s_j}$ is the Kronecker delta. Using periodic boundary conditions, the microstructure evolves via a Monte-Carlo technique in which a lattice site is selected at random and a new orientation is randomly specified for the lattice site. If the switch leads to a decrease in energy ($\Delta H < 0$), the reorientation is accepted. Each reorientation attempt corresponds to $\frac{1}{N_s}$ Monte-Carlo steps (MCS). For the purposes of generating the microstructures, a 91125 lattice point grid was utilized with microstructures generated for 1000 MCS.

C.2. Pore structure of tungsten

Realistic pore structures of tungsten were obtained by adapting a Monte-Carlo method proposed by Aldazabal et al. [17]. For the experimental microstructure used for reconstruction (Fig. 8), the liquid matrix obtained from the simulation is replaced with the Silver matrix. An initial microstructure is created using random seeds of solid particles in a liquid matrix over a N_s lattice site 3D model. Lattice sites are regarded as 3D voxels with face and edge neighbors. Solidification occurs at the surface of fluid-solid interface and is modeled by assigning weights ($J_i, i = 1,\ldots,18$) to the face and edge solid neighbors. Each solid edge neighbor is given a weight of $\frac{1}{\sqrt{2}}$ and each solid face neighbor is assigned a weight of 1. The switching of phases is done by calculating the sum of the weights of the neighbors ($\sum J_i$) of a selected voxel. To model the energetic favorability of the solidification of a liquid voxel, the following probability (P) rule is used,

$$P = \begin{cases} 1 & \text{if } \sum J_i \geqslant 8.6568, \\ 0.01 & \text{if } 3.8284 \leqslant \sum J_i < 8.6568, \\ 0 & \text{if } \sum J_i < 3.8284. \end{cases} \tag{C.2}$$

A linear probability distribution is used to solidify the voxels according to the solvent concentration. Solute concentration gradients are modeled by Fick's law using a finite difference scheme over the lattice after a series of MCS.

References

[1] M.S. Talukdar, O. Torsaeter, M.A. Ioannidis, J.J. Howard, Stochastic reconstruction, 3D characterization and network modeling of chalk, J. Petrol. Sci. Eng. 35 (1–2) (2002) 1–21.
[2] A.P. Roberts, E.J. Garboczi, Elastic properties of a tungsten-silver composite by reconstruction and computation, J. Mech. Phys. Solids. 47 (1999) 2029–2055.
[3] J. Fleig, J. Maier, The influence of laterally inhomogeneous contacts on the impedance of solid materials: A three-dimensional finite-element study, J. Electroceram. 1 (1) (1997) 73–89.
[4] G. Dotelli, I.N. Lora, C. Schmid, C.M. Mari, Composite materials as electrolytes for solid oxide fuel cells: simulation of microstructure and electrical properties, Solid State Ionics 152–153 (2002) 509–515.
[5] L.O.E. Santos, P.C. Philippi, M.C. Damiani, C.P. Fernandes, Using three-dimensional reconstructed microstructures for predicting intrinsic permeability of reservoir rocks based on a Boolean lattice gas method, J. Petrol. Sci. Eng. 35 (1–2) (2002) 109–124.
[6] B. Bochenek, R. Pyrz, Reconstruction of random microstructures—a stochastic optimization problem, Comput. Mater. Sci. 31 (1–2) (2004) 93–112.
[7] J.A. Quiblier, A new three-dimensional modeling technique for studying porous media, J. Colloid Interface Sci. 98 (1984) 84–102.
[8] P.M. Adler, C.G. Jacquin, J.A. Quiblier, Flow in simulated porous media, Int. J. Multiphase Flow. 16 (4) (1990) 691–712.
[9] R.D. Hazlett, Statistical characterization and stochastic modelling of pore networks in relation to fluid flow, Math. Geol. 29 (1997) 801–822.
[10] C.L.Y. Yeong, S. Torquato, Reconstructing random media II. Three-dimensional media from two-dimensional cuts, Phys. Rev. E. 58 (1) (1998) 224–233.
[11] B. Biswal, R. Hilfer, Microstructure analysis of reconstructed porous media, Physica A 266 (1999) 307–311.
[12] P-E. Øren, S. Bakke, Reconstruction of Berea sandstone and pore-scale modelling of wettability effects, J. Petrol. Sci. Eng. 39 (3–4) (2003) 177–199.
[13] I.F. Vasconcelos, I. Cantat, J.A. Glazier, Dynamics and topological aspects of a reconstructed two-dimensional foam time series using Potts Model on a pinned lattice, J. Comput. Phys. 192 (2003) 1–20.
[14] Z. Liang, M.A. Ioannidis, I. Chatzis, Permeability and electrical conductivity of porous media from3D stochastic replicas of the microstructure, Chem. Eng. Sci. 55 (22) (2000) 5247–5262.

[15] B. Biswal, C. Manwart, R. Hilfer, S. Bakke, P.-E. Øren, Quantitative analysis of experimental and synthetic microstructures for sedimentary rock, Physica A 273 (1999) 452–475.
[16] M.P. Anderson, D.J. Srolovitz, G.S. Grest, P.S. Sahni, Computer simulation of grain growth I. Kinetics, Acta Metall. 32 (5) (1984) 783–791.
[17] J. Aldazabal, A. Martin-Meizoso, J.M. Martinez-Esnaola, Simulation of liquid phase sintering using the Monte-Carlo method, Mater. Sci. Eng. A 365 (1–2) (2004) 151–155.
[18] S. Dumais, Using SVMs for text categorization, IEEE Intell. Syst. 13 (4) (1998) 21–23.
[19] M. Pontil, A. Verri, Support vector machines for 3D object recognition, IEEE Trans. Pattern Anal. Mach. Intell. 20 (6) (1998) 637–646.
[20] S. Li, J.T. Kwok, H. Zhu, Y. Wang, Texture classification using the support vector machines, Pattern Recogn. 36 (2003) 2883–2893.
[21] N.J. Wittridge, R.D. Knutsen, A microtexture based analysis of the surface roughening behaviour of an aluminium alloy during tensile deformation, Mater. Sci. Eng. A 269 (1–2) (1999) 205–216.
[22] G.F. Vander Voort, Metallography: principles and practice, McGraw-Hill Book Company, New York, 1984.
[23] K. Mehnert, J. Ohser, P. Klimanek, Testing stereological methods for the estimation of spatial size distributions by means of computer-simulated grain structures, Mater. Sci. Eng. A 246 (1998) 207–212.
[24] J. Ohser, F. Múcklich, Statistical Analysis of Microstructures in Materials Science, first ed., John Wiley and Sons, New York, 2000.
[25] G.W. Milton, N. Phan-Thien, New bounds on effective elastic moduli of two-component materials, Proc. Roy. Soc. London A 380 (1982) 305–331.
[26] M. Beran, J. Molyneux, Use of classical variational principles to determine bounds for the effective bulk modulus in heterogeneous media, Q. Appl. Math. 24 (1966) 107–118.
[27] Z. Hashin, S. Shtrikman, A variational approach to the theory of the elastic behaviour of multi-phase materials, J. Mech. Phys. Solids. 11 (1963) 127–140.
[28] J. Quintanilla, Microstructure and properties of random heterogeneous materials: A review of theoretical results, Poly. Engg. Sci. 39 (1999) 559–585.
[29] S. Umekawa, R. Kotfila, O.D. Sherby, Elastic properties of a tungsten-silver composite above and below the melting point of silver, J. Mech. Phys. Solids 13 (4) (1965) 229–230.
[30] M. Turk, A. Pentland, Eigenfaces for recognition, Int. J. Cogn. Neurosci. 3 (1) (1991) 71–86.
[31] L. Sirovich, M. Kirby, Low-dimensional procedure for the characterization of human faces, J. Opt. Soc. Am 4 (1987) 519–524.
[32] V. Sundararaghavan, N. Zabaras, A dynamic material library for the representation of single phase polyhedral microstructures, Acta Materialia 52 (14) (2004) 4111–4119.
[33] V.N. Vapnik, Statistical Learning Theory, Wiley, New York, 1998.
[34] C.C. Chang, C.J. Lin, LIBSVM: a library for support vector machines (2001) www.csie.ntu.edu.tw/~cjlin/libsvm.
[35] A.P. Roberts, S. Torquato, Chord-distribution functions of three-dimensional random media: Approximate first-passage times of Gaussian processes, Phys. Rev. E. 59 (5) (1999) 4953–4963.
[36] C. Manwart, R. Hilfer, Reconstruction of random media using Monte-Carlo methods, Phys. Rev. E. 59 (1999) 5596–5599.
[37] C. Manwart, S. Torquato, R. Hilfer, Stochastic reconstruction of sandstones, Phys. Rev. E. 62 (2000) 893–899.
[38] B. Lu, S. Torquato, *N*-point probability functions for a lattice model of heterogeneous media, Phys. Rev. B. 42 (7) (1990) 4453–4459.
[39] E.J. Garboczi, NIST Internal Report 6269, (1998) www.ciks.cbt.nist.gov/garboczi/, Chapter 2.
[40] S. Ganapathysubramanian, N. Zabaras, On the synergy between classification of textures and process sequence selection, in: M.E. Schlesinger, (Ed), The proceedings of EPD Congress, 2004, The Minerals, Metals and Materials Society, Charlotte, 2004.
[41] S. Torquato, Random heterogeneous media: microstructure and improved bounds on effective properties, Appl. Mech. Rev. 44 (1991) 37–76.